Observation of a Topological Edge State Stabilized by Dissipation

Helene Wetter,[1] Michael Fleischhauer,[2] Stefan Linden,[1] and Julian Schmitt[3,*]
[1]Physikalisches Institut, Universität Bonn, Nussallee 12, 53115 Bonn, Germany
[2]Department of Physics and Research Center OPTIMAS, RPTU Kaiserslautern-Landau, 67663 Kaiserslautern, Germany
[3]Institut für Angewandte Physik, Universität Bonn, Wegelerstrasse 8, 53115 Bonn, Germany

(Received 15 March 2023; accepted 20 July 2023; published 24 August 2023)

Robust states emerging at the boundary of a system constitute a hallmark for topological band structures. Other than in closed systems, topologically protected states can occur even in systems with a trivial band structure, if exposed to suitably modulated losses. Here, we study the dissipation-induced emergence of a topological band structure in a non-Hermitian one-dimensional lattice system, realized by arrays of plasmonic waveguides with tailored loss. We obtain direct evidence for a topological edge state that resides in the center of the band gap. By tuning dissipation and hopping, the formation and breakdown of an interface state between topologically distinct regions is demonstrated.

DOI: 10.1103/PhysRevLett.131.083801

Topology is an important paradigm for our understanding of phases of matter [1], with the quantum Hall effect constituting a prominent example of a topological system isolated from the environment [2]. Interfacing materials with distinct topological properties has remarkable implications leading to localized edge states at the boundary, which due to their robustness against disorder are considered as valuable resource states for quantum technologies [3]. Conceptually, the robustness results from the existence of global integer-valued invariants, which can only change in a phase transition associated with the closing of a gap. Inspired by solid-state systems, topological states in closed Hermitian systems have been experimentally realized in a wide range of platforms, such as ultracold atoms or photonics [4–6].

Exploring topological phenomena in open systems presents a complementary approach to realize robust edge states, where the coupling between the system and the environment (e.g., by pumping or dissipation of particles) acts as a resource rather than a limitation. Starting from the prediction of topological transitions in non-Hermitian quantum walk [7], conceptual questions about the classification of open-system topological phases for non-Hermitian and Lindbladian settings [8–12], the role of topological invariants and edge states [13–18], and the band theory [19,20] have been addressed theoretically. Experimentally, non-Hermitian systems have been realized in photonics, where driven-dissipative effects can be engineered [21]. Combining topologically nontrivial photonic crystals with gain or loss, this has allowed for the observation of topological (lasing) states in waveguides [22,23], resonator arrays [24,25], and exciton-polaritons [26,27]. Topological protection is here, however, inherited from the photonic band structure, and not from a coupling to reservoirs. The implementation of topological phases that solely arise from non-Hermiticity and lack a Hermitian counterpart, as proposed in Refs. [8,9,28,29] and realized with mechanical metamaterials [30], acoustic cavities [31,32], and electrical circuits [33], has so far remained elusive for optical systems.

In this Letter, we report measurements of light-matter states with nontrivial topological properties, solely induced by tailored dissipation. Using surface plasmon polaritons (SPPs) confined in waveguide arrays, we obtain signatures for open-system topological edge states by identifying zero-energy modes localized at the boundary of the sample. The underlying one-dimensional (1D) lattice with four-site unit cell realizes a non-Hermitian extension of the paradigmatic Su-Schrieffer-Heeger (SSH) model [34], despite uniform hopping throughout the lattice. By tuning dissipation and hopping, the birth and death of a non-Hermitian topologically protected edge state is demonstrated.

The basic principle of our topological system [see Fig. 1(a)] relies on a 1D lattice with spatially uniform nearest-neighbor hopping J and spatially varying dissipation at the lattice sites [28,29]. The unit cell consists of four sites spaced by d, which are subject to a gain-loss pattern $(ig_1, -ig_2, -ig_1, ig_2)$ with real-valued dimensionless amplitudes $g_{1,2}$. The Bloch Hamiltonian of the open system at wave vector k_x

$$\hat{H}_{k_x} = J\begin{pmatrix} ig_1 & 1 & 0 & e^{-4ik_x d} \\ 1 & -ig_2 & 1 & 0 \\ 0 & 1 & -ig_1 & 1 \\ e^{4ik_x d} & 0 & 1 & ig_2 \end{pmatrix} - iJg_0\mathbb{1} \qquad (1)$$

is a non-Hermitian matrix, i.e., $\hat{H} \neq \hat{H}^\dagger$, with complex energy eigenvalues E. Here, $g_0 > 0$ accounts for a loss at all lattice sites, which governs our implementation using

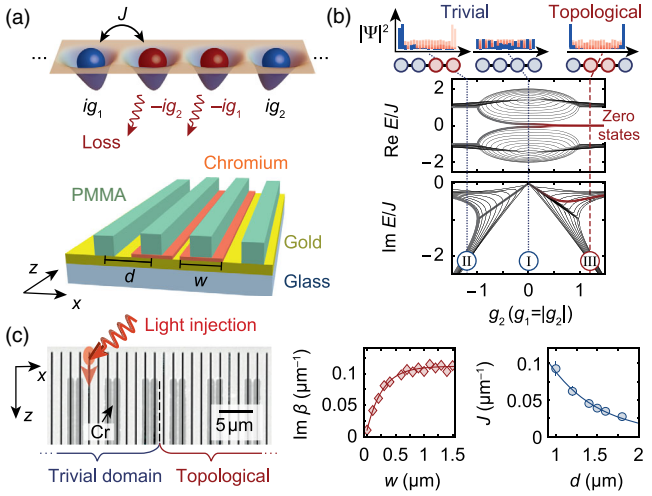

FIG. 1. Experimental scheme. (a) Lattice system with nontrivial topology induced solely by dissipation (top) and experimental realization with DLSPPWs spaced by distance d, where losses are induced by chromium stripes of width w (bottom). (b) Complex-valued energy spectrum for 40 lattice sites with $g_1 = |g_2|$. For $g_2 < 0$, the system is topologically trivial and the probability density $|\Psi|^2$ is concentrated in the first two lattice sites (top left). In the topologically nontrivial regime ($g_2 > 0$), $|\Psi|^2$ is exponentially localized at the edges (top right) and associated with midgap states at zero energy (red lines). (c) Left: Waveguide sample with chromium stripes (dark gray) arranged to realize trivial (topological) domains in the left (right) sample half. The chromium-free region on top is used to excite the waveguides by grating coupling of laser light. Right: Measured dissipation in a single waveguide Imβ versus w and hopping J between two waveguides versus d, along with fits (lines).

purely dissipative waveguides; see Fig. 1(a) (bottom). Because of the global loss the steady state is here the trivial vacuum. Nevertheless, as we will demonstrate in our experiments, the system possesses a nontrivial nonequilibrium topology, protected by the symmetries of the Liouvillian $\mathcal{L}$ that governs the dynamics of the density matrix ρ, according to $\dot{\rho} = \mathcal{L}\rho$ [12]. The dynamical generators fulfill time reversal (T), charge-conjugation (C), and chiral (S) symmetries [35], characterizing the class BDI [1], which can have a nontrivial topology in 1D.

The topological character of the four-site model becomes apparent when considering the energy band structure and eigenstates in a finite-length lattice for different loss patterns, as shown in Fig. 1(b); for simplicity, we consider the symmetric case $g_1 = |g_2|$ and $g_0 = |g_2|$ with g_2 as the control parameter. In the different parameter regimes, $\mathrm{diag}(\hat{H}) = (0,0,0,0)$ for $g_2 = 0$ (lossless trivial, I), $\mathrm{diag}(\hat{H}) = -2iJ|g_2|(0,0,1,1)$ for $g_2 < 0$ (dissipative trivial, II), and $\mathrm{diag}(\hat{H}) = -2iJg_2(0,1,1,0)$ for $g_2 > 0$ (topologically nontrivial, III), respectively [blue and red circles in Fig. 1(b)]. Phase (I) exhibits a metallike gapless band structure with probability densities $|\Psi|^2$ delocalized in the bulk, while the band structure in phase (II) is gapped. In striking contrast, phase (III) features two midgap states at zero energy in ReE (red lines), which are localized at the boundary of the system and decay exponentially into the bulk. Because of the dissipative nature of the system, Im$E < 0$ for all states. Note that while there is not yet a general understanding of nonequilibrium invariants for density matrices, a topological number for the non-Hermitian system has been identified theoretically as a global Berry phase, which takes discrete values $W = 0$ or 1 for $g_1 g_2 < 0$ or $g_1 g_2 > 0$ in phases (II) or (III), respectively [14,28]; for details, see Ref. [35]. Based on the nonequilibrium symmetries [35] and the above mentioned spectral and spatial signatures, topological states solely induced by dissipation rather than Hermitian band engineering are theoretically expected in our system.

To experimentally investigate the topological properties of the non-Hermitian lattice system, we utilize SPPs confined in evanescently coupled arrays of dielectric loaded SPP waveguides (DLSPPWs) with tailored losses. The samples are fabricated by two-step electron beam lithography [35,39]. Figure 1(a) (bottom) outlines a typical waveguide structure, realized by depositing polymethyl methacrylate (PMMA) ridges of about 200 nm width and center-to-center spacing d on top of a glass substrate, previously coated with a low-absorption 60 nm-thin gold layer to host the plasmonic part of the polaritons. Losses at individual lattice sites are introduced and controlled by adding chromium stripes of variable width w below the ridges.

An exemplary sample containing two different loss patterns in the unit cells, corresponding to the topologically trivial (II) and nontrivial (III) region, is shown in Fig. 1(c). The SPP evolution in the array is excited with a 980 nm laser at 15 μW optical power and characterized by leakage radiation microscopy [6,35]. By varying w and d, both the additional absorption Imβ from chromium and the hopping J (both in units $\mu\mathrm{m}^{-1}$) can be accurately controlled; see Fig. 1(c) (right). Here, β denotes the complex-valued propagation constant in a single waveguide [6]. In terms of Eq. (1), the dissipation parameters follow as $g_2 = \mathrm{Im}\beta/(2J)$.

First, we study the evolution of the SPPs upon injecting a wave packet at the edge and in the bulk of the waveguide arrays, respectively, for three loss patterns according to phases (I) (metallike), (II) (dissipative trivial), and (III) (dissipative topological). Figure 2(a) shows the real-space SPP intensity distributions obtained by imaging the leakage radiation [35]. For phase (I) [Fig. 2(a), left column], the SPP evolution mimics a two-state quantum walk of a particle in a periodic potential. This metallike behavior is highlighted by a conical transport along with a characteristic interference pattern when injecting the wave packet in the bulk; upon injection at the edge, the wave packet simply propagates in the $-x$ direction. With losses as in the topologically trivial phase (II) [Fig. 2(a), middle], the ballistic transport is inhibited and an oscillation of the intensity between two neighboring low-loss waveguides is

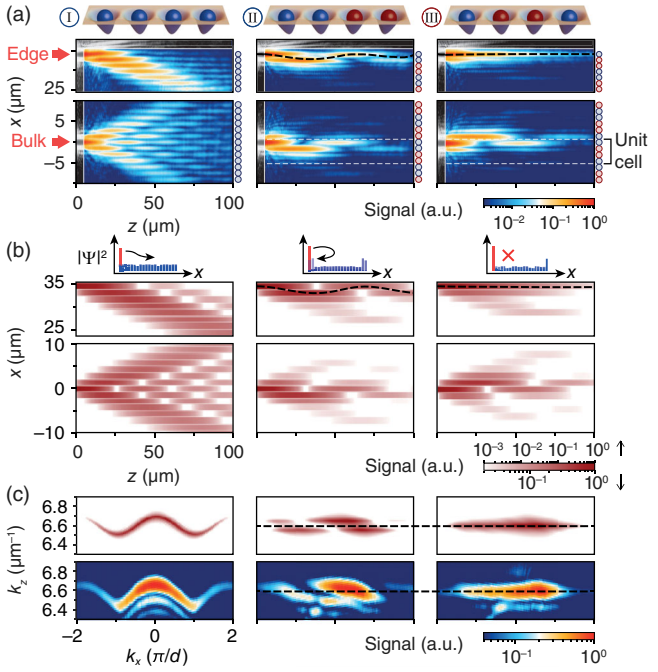

FIG. 2. SPP evolution for metallike (left, I), dissipative topologically trivial (middle, II), and dissipation-induced topological domains (right, III). (a) Real-space intensity distribution for injection at the edge (top) and at the first site of a unit cell in the bulk (bottom), for a sample of 48 waveguides spaced by $d = 1.4$ μm, corresponding to $J = 0.045(3)$ μm^{-1}. Solid and white dashed lines indicate sample boundaries and unit cells, and black dashed lines give the center of mass. For the used $w = 0.7$ μm in (II) and (III), Im$\beta = 0.1$ μm^{-1}, and $g_1 = |g_2| = 1.1$. (b) Simulated intensity evolution in the arrays from (a) with $J = 0.045$ μm^{-1} and Im$\beta = 0.1$ μm^{-1} for the lossy [red in (a)] and Im$\beta = 0.01$ μm^{-1} for the low-loss [blue in (a)] waveguides, in good agreement with the experimental results. (c) Momentum-resolved energy spectra with cos-shaped band for bulk excitation, band gap in the trivial, and flat band in the topological domains, respectively, for edge excitation [35], along with theory prediction (top). Dashed lines indicate the energy of the topological zero mode (right), which lies between the bulk bands of case (II) (middle).

observed for both excitation protocols. In contrast, with losses as in the topologically nontrivial phase (III) [Fig. 2(a), right], the edge excitation reveals apart from the overall damping a quasistationary intensity evolution that remains locked to the outermost waveguide. This localization occurs at the edge only, as understood from the corresponding probability density $|\Psi|^2$ shown in Fig. 1(b) (top), while excitation in the bulk reveals the same oscillatory dynamics as in phase (II), except for a phase shift due to the neighboring low-loss waveguide now lying above the excited one. The oscillation results from a beating between bonding and antibonding states in the hybridized neighboring lattice sites [Fig. 2(c)]. In contrast, the absence of a beating indicates the zero energy of the topological edge state. The phenomenology observed in the measured real-space intensity is in good agreement with numerical simulations based on coupled mode theory [35] [see Fig. 2(b)], giving conclusive evidence that the non-Hermitian model is well-captured by our DLSPPW platform.

Figure 2(c) shows the momentum-resolved occupation of the energy bands within the first two Brillouin zones from $k_x = -2\pi/d$ to $2\pi/d$, as obtained by recording the leakage radiation in the back-focal Fourier plane of the microscope objective [35]. In the metallike phase (I) and for bulk excitation, the spectrum matches the expected cos-shaped energy band that complements the independently observed ballistic transport in real space. The spectrum agrees with the simulated one in Fig. 2(c), except for a circular segment at $k_z \lesssim 6.5$ μm^{-1} that is well understood to arise from unconfined SPP propagation outside of the array [40], also visible in the gray shaded area in Fig. 2(a). In the dissipative topologically trivial phase (II) and for edge excitation, the momentum distribution considerably changes. Two energy bands separated by a gap near $k_z = 6.56(2)$ μm^{-1} and visible at $k_x \approx -0.5\pi/d$ are observed. In the topologically nontrivial phase (III), on the other hand, the momentum distribution exhibits only a single flat energy band centered at $k_z = 6.59(2)$ μm^{-1}, with a spectral width determined by losses and residual transport in the bulk. By comparing with Fig. 1(b), the data gives evidence for a topological zero state in the band gap.

A unique feature of the investigated system lies in the fact that topological properties emerge as a consequence of dissipation alone, in a lattice which would be otherwise topologically trivial. To systematically test this dissipation-induced birth of topological order, we focus on an interface between two distinct domains prepared in phases (II) and (III), respectively, and gradually increase the loss Imβ. Figure 3(a) shows the real-space SPP evolution for increasing chromium widths w, after consistently exciting the same low-loss waveguide, which is located at the interface. The conical intensity spread into the bulk for $w = 0$, previously seen in Fig. 2, is gradually transformed into a quasistationary, i.e., transversely localized occupation of the interface waveguide. Remarkably, despite larger absorption Imβ, the SPP propagation length is significantly enhanced. This is understood from the increase of ImE for the topological zero states for large enough $g_2 \gtrsim 0.7$ [see Fig. 1(b) (bottom panel, red line)], marking a clear distinction point from its more lossy topologically trivial counterpart in a phase-(II) system for $g_2 < 0$ [Fig. 1(b) (bottom panel, gray line)]. Thus, the intensity becomes more localized and long-lived at the interface due to the presence of topologically distinct domains. The extended propagation distance is visually more striking in the line profiles at $z = 50$ μm in Fig. 3(b). Quantitatively, Fig. 3(c) shows the fitted $1/e$ decay length of the intensity at the interface as a function of w, along with the theoretically expected decay length at the interface waveguide and in

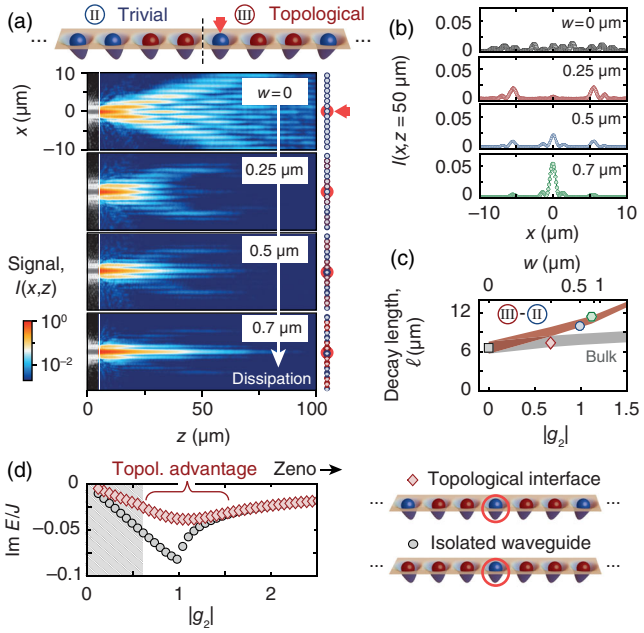

FIG. 3. Dissipation-induced emergence of interface state between distinct topological domains. (a) Interface between phase-(II) and phase-(III) domains realized by different loss patterns, and real-space intensity distribution $I(x,z)$ upon excitation of the interface waveguide (red) for increasing losses $\mathrm{Im}\beta = \{0, 0.06, 0.09, 0.1\}$ μm^{-1} from larger chromium widths w. Losses correspond to $g_1 = |g_2| = \{0, 0.7, 1, 1.1\}$ and, as before, $J = 0.045(3)$ μm^{-1}. (b) Line profiles of the intensity averaged around $z = 50$ μm. (c) Decay length ℓ of intensity in interface waveguide for cases in (a); for fitted line profiles $I(x = 0, z)$, see Ref. [35]. Despite increased chromium absorption, an enhanced propagation distance is observed, providing evidence for a topologically robust state. Shaded areas show simulations for the interface (red) and bulk (gray), where the enhanced ℓ indicates the interface robustness beyond $g_2 \approx 0.7$. (d) Advantage of topological interface over isolated waveguide, seen in reduction of calculated ImE when induced losses and hopping are of the same order $g_2 \sim 1$. For small g_2 (shaded) the edge state delocalizes, for large g_2 Zeno-like decoupling dominates.

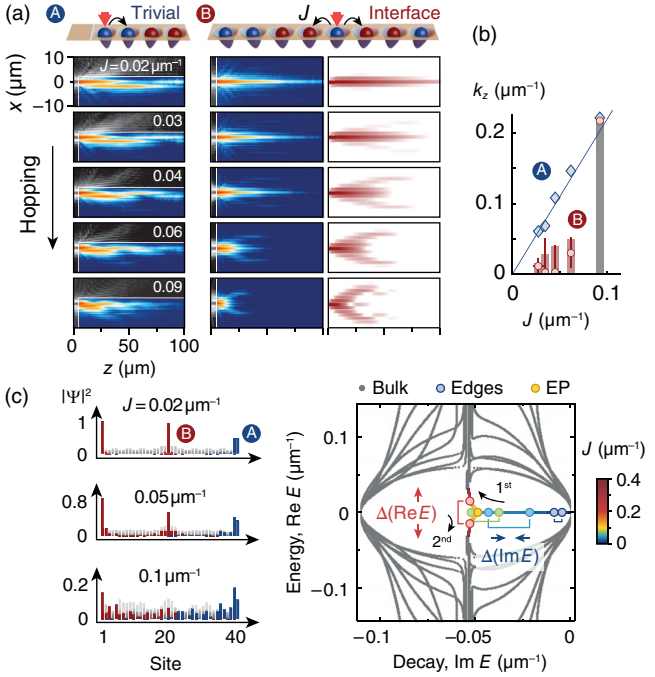

FIG. 4. Breaking the topological protection at an exceptional point. (a) SPP evolution for increasing hopping J, realized by reduced waveguide spacings $d = \{1.8, 1.6, 1.4, 1.2, 1.0\}$ μm at $w = 0.7$ μm ($\mathrm{Im}\beta = 0.1$ μm^{-1}). For excitation at the trivial edge (A), the population oscillates faster as J increases. Upon injecting light into the (II)-(III) interface (B), a quasistationary edge state is observed, which at $J \approx 0.09$ μm^{-1} becomes delocalized in the bulk, in agreement with simulations (right). (b) Oscillation frequency k_z at excited waveguide fitted with $I(z) = a_1 \cos(k_z z + \phi) e^{-z/\ell} + a_0$. Solid line and bars give numerical results, and error bars denote uncertainties of fit parameter. (c) Left: Calculated probability density at boundaries, along with bulk modes (gray). A delocalization of the interface mode (red) is visible for too large J, indicating the loss of topological character. Right: Complex eigenenergies of the two topological (colored) and 38 bulk (gray) states, as J is varied. For $J \approx 0.095$ μm^{-1}, the eigenvalues coalesce at an exceptional point (yellow).

the bulk, confirming the genuine dissipation-enhanced topological robustness of the interface state. To emphasize the effect of topology, Fig. 3(d) shows calculations in which we compare ImE of the topological interface state to that of a mode localized at an isolated low-loss waveguide embedded in a bulk of lossy waveguides. In an intermediate regime where losses and hopping are of the same order, $0.6 \lesssim g_2 \lesssim 1.5$, a smaller absorption is observed for the topological configuration. This means that light transport along an interface between distinct topological domains is indeed expected to be enhanced. For larger values of g_2, Zeno-like decoupling dominates and both configurations show essentially the same losses.

Conversely to the discussed formation of an edge state upon introducing dissipation, we next focus on *breaking* the topological protection at the interface by increasing the hopping J in the presence of dissipation. For this, we have reduced the waveguide spacing d, while keeping the losses in the interfaced phases (II) and (III) fixed at $\mathrm{Im}\beta = 0.1$ μm^{-1} [with $w = 0.7$ μm as in Fig. 2]. Figure 4(a) shows the real-space SPP evolution after injection of a wave packet at the boundary between a trivial phase-(II) domain and the vacuum. Not surprisingly, the population oscillates between the two low-loss waveguides as before, but now with a larger wave vector k_z as J is increased; see the blue data in Fig. 4(b). At the phase (II)-(III) interface shown in Fig. 4(a), the SPP population stays localized at the interface waveguide without any appreciable transverse transport or oscillation; see the red data in Fig. 4(b). Eventually, at $J \approx 0.09$ μm^{-1}, the tunnel coupling becomes so large that the SPPs propagate away from the interface into the bulk, breaking up the topological edge state.

The diminished topological protection is understood to result from a delocalization of the interface mode with increased J, as shown in Fig. 4(c). The calculated $|\Psi|^2$ is shown for the trivial edge and interface modes, along with bulk modes. For larger J, we find the transverse localization length of the interface mode to extend further, revealing an exponential decay of $|\Psi|^2$ into the bulk with a maximum probability that consistently occurs at the interface waveguide. For the trivial edge, however, the maximum of the probability soon shifts away from the boundary of the sample and generally does not exhibit an exponential decay toward the bulk region. This phenomenology shares a close analogy with the topological edge states encountered in the SSH model [34], where the probability density of the dimerized edge modes decays exponentially. In the non-Hermitian four-site model, the alternating hopping of the SSH model is replaced by an effective (de)coupling of pairs of gain-gain or loss-loss (mixed gain-loss) lattice sites [28], and a dimerization with two- and four-site periodicity occurs in $\mathrm{Re}\Psi$ and $\mathrm{Im}\Psi$, respectively.

Finally, the spectrum of the complex energy eigenvalues in Fig. 4(c) provides a physical picture about the broken topological protection of the interface state (colored circles; energies of bulk modes are shown in gray) near $J \approx 0.095\ \mu\mathrm{m}^{-1}$. For small J, the eigenvalues of the zero states with $\mathrm{Re}E = 0$ fall in the band gap and are separated in $\mathrm{Im}E$ (blue, green circles); note that due to $\mathrm{Im}E \neq 0$ the non-Hermitian system is not $\mathcal{PT}$-symmetric [21]. As J increases, the imaginary gap closes and the eigenvalues coalesce at an exceptional point (yellow circle), followed by an opening of a real energy gap, which lifts the edge state degeneracy and merges both with the bulk bands, visible in Fig. 4(c) (red circle). At the exceptional point, the system has lost its topological character.

In conclusion, we have experimentally demonstrated open-system topological states induced by dissipation alone, using SPP waveguide arrays with uniform hopping and spatially distributed loss. Evidence for the topological nature of the non-Hermitian system is obtained from a localized midgap edge state between distinct topological domains. By independently tuning dissipation and hopping, both the emergence and breaking of topological order is observed. For the future, lowering the SPP losses may enable direct measurements of the topological invariant by interferometry [41] and give access to non-Hermitian Floquet engineering by modulated loss and hopping [39,42]. An intriguing perspective lies in the implementation of open-system topological states with optical quantum gases within optically active microcavities [43,44], opening ways to study the fate of topological order in the presence of fluctuations in one and two dimensions [18,45]. In combination with gain, dissipation-induced topological edge states are also interesting candidates for applications such as robust routing of light in reconfigurable interface channels, e.g., for optical interconnects.

We thank V. Zimmermann and Z. Fedorova for discussions. S. L., M. F., and J. S. acknowledge support from the DFG within SFB/TR 185 (277625399). J. S. acknowledges support by the EU (ERC, TopoGrand, 101040409), and by DFG within the Cluster of Excellence ML4Q (EXC 2004/1–390534769).

*Corresponding author: schmitt@iap.uni-bonn.de

[1] A. Altland and M. R. Zirnbauer, Nonstandard symmetry classes in mesoscopic normal-superconducting hybrid structures, Phys. Rev. B **55**, 1142 (1997).
[2] K. v. Klitzing, G. Dorda, and M. Pepper, New Method for High-Accuracy Determination of the Fine-Structure Constant Based on Quantized Hall Resistance, Phys. Rev. Lett. **45**, 494 (1980).
[3] S. D. Sarma, M. Freedman, and C. Nayak, Majorana zero modes and topological quantum computation, npj Quantum Inf. **1**, 15001 (2015).
[4] S. de Léséleuc, V. Lienhard, P. Scholl, D. Barredo, S. Weber, N. Lang, H. P. Büchler, T. Lahaye, and A. Browaeys, Observation of a symmetry-protected topological phase of interacting bosons with Rydberg atoms, Science **365**, 775 (2019).
[5] T. Ozawa, H. M. Price, A. Amo, N. Goldman, M. Hafezi, L. Lu, M. C. Rechtsman, D. Schuster, J. Simon, O. Zilberberg, and I. Carusotto, Topological photonics, Rev. Mod. Phys. **91**, 015006 (2019).
[6] F. Bleckmann, Z. Cherpakova, S. Linden, and A. Alberti, Spectral imaging of topological edge states in plasmonic waveguide arrays, Phys. Rev. B **96**, 045417 (2017).
[7] M. S. Rudner and L. S. Levitov, Topological Transition in a Non-Hermitian Quantum Walk, Phys. Rev. Lett. **102**, 065703 (2009).
[8] C.-E. Bardyn, M. A. Baranov, C. V. Kraus, E. Rico, A. İmamoğlu, P. Zoller, and S. Diehl, Topology by dissipation, New J. Phys. **15**, 085001 (2013).
[9] D. Linzner, L. Wawer, F. Grusdt, and M. Fleischhauer, Reservoir-induced Thouless pumping and symmetry-protected topological order in open quantum chains, Phys. Rev. B **94**, 201105(R) (2016).
[10] Z. Gong, Y. Ashida, K. Kawabata, K. Takasan, S. Higashikawa, and M. Ueda, Topological Phases of Non-Hermitian Systems, Phys. Rev. X **8**, 031079 (2018).
[11] S. Lieu, M. McGinley, and N. R. Cooper, Tenfold Way for Quadratic Lindbladians, Phys. Rev. Lett. **124**, 040401 (2020).
[12] A. Altland, M. Fleischhauer, and S. Diehl, Symmetry Classes of Open Fermionic Quantum Matter, Phys. Rev. X **11**, 021037 (2021).
[13] H. Schomerus, Topologically protected midgap states in complex photonic lattices, Opt. Lett. **38**, 1912 (2013).
[14] S.-D. Liang and G.-Y. Huang, Topological invariance and global Berry phase in non-Hermitian systems, Phys. Rev. A **87**, 012118 (2013).
[15] D. Leykam, K. Y. Bliokh, C. Huang, Y. D. Chong, and F. Nori, Edge Modes, Degeneracies, and Topological Numbers in Non-Hermitian Systems, Phys. Rev. Lett. **118**, 040401 (2017).

[16] S. Yao and Z. Wang, Edge States and Topological Invariants of Non-Hermitian Systems, Phys. Rev. Lett. **121**, 086803 (2018).
[17] F. K. Kunst, E. Edvardsson, J. C. Budich, and E. J. Bergholtz, Biorthogonal Bulk-Boundary Correspondence in Non-Hermitian Systems, Phys. Rev. Lett. **121**, 026808 (2018).
[18] X.-W. Luo and C. Zhang, Higher-Order Topological Corner States Induced by Gain and Loss, Phys. Rev. Lett. **123**, 073601 (2019).
[19] H. Shen, B. Zhen, and L. Fu, Topological Band Theory for Non-Hermitian Hamiltonians, Phys. Rev. Lett. **120**, 146402 (2018).
[20] K. Yokomizo and S. Murakami, Non-Bloch Band Theory of Non-Hermitian Systems, Phys. Rev. Lett. **123**, 066404 (2019).
[21] L. Feng, R. El-Ganainy, and L. Ge, Non-Hermitian photonics based on parity–time symmetry, Nat. Photonics **11**, 752 (2017).
[22] J. M. Zeuner, M. C. Rechtsman, Y. Plotnik, Y. Lumer, S. Nolte, M. S. Rudner, M. Segev, and A. Szameit, Observation of a Topological Transition in the Bulk of a Non-Hermitian System, Phys. Rev. Lett. **115**, 040402 (2015).
[23] S. Weimann, M. Kremer, Y. Plotnik, Y. Lumer, S. Nolte, K. G. Makris, M. Segev, M. C. Rechtsman, and A. Szameit, Topologically protected bound states in photonic parity–time-symmetric crystals, Nat. Mater. **16**, 433 (2017).
[24] B. Bahari, A. Ndao, F. Vallini, A. E. Amili, Y. Fainman, and B. Kanté, Nonreciprocal lasing in topological cavities of arbitrary geometries, Science **358**, 636 (2017).
[25] H. Zhao, P. Miao, M. H. Teimourpour, S. Malzard, R. El-Ganainy, H. Schomerus, and L. Feng, Topological hybrid silicon microlasers, Nat. Commun. **9**, 981 (2018).
[26] P. St-Jean, V. Goblot, E. Galopin, A. Lemaître, T. Ozawa, L. Le Gratiet, I. Sagnes, J. Bloch, and A. Amo, Lasing in topological edge states of a one-dimensional lattice, Nat. Photonics **11**, 651 (2017).
[27] S. Klembt, T. H. Harder, O. A. Egorov, K. Winkler, R. Ge, M. A. Bandres, M. Emmerling, L. Worschech, T. C. H. Liew, M. Segev, C. Schneider, and S. Höfling, Exciton-polariton topological insulator, Nature (London) **562**, 552 (2018).
[28] K. Takata and M. Notomi, Photonic Topological Insulating Phase Induced Solely by Gain and Loss, Phys. Rev. Lett. **121**, 213902 (2018).
[29] P. Comaron, V. Shahnazaryan, W. Brzezicki, T. Hyart, and M. Matuszewski, Non-Hermitian topological end-mode lasing in polariton systems, Phys. Rev. Res. **2**, 022051(R) (2020).
[30] H. Fan, H. Gao, S. An, Z. Gu, S. Liang, Y. Zheng, and T. Liu, Hermitian and non-Hermitian topological edge states in one-dimensional perturbative elastic metamaterials, Mech. Syst. Signal Process. **169**, 108774 (2022).
[31] H. Gao, H. Xue, Q. Wang, Z. Gu, T. Liu, J. Zhu, and B. Zhang, Observation of topological edge states induced solely by non-Hermiticity in an acoustic crystal, Phys. Rev. B **101**, 180303(R) (2020).
[32] H. Gao, H. Xue, Z. Gu, T. Liu, J. Zhu, and B. Zhang, Non-Hermitian route to higher-order topology in an acoustic crystal, Nat. Commun. **12**, 1888 (2021).
[33] S. Liu, S. Ma, C. Yang, L. Zhang, W. Gao, Y. J. Xiang, T. J. Cui, and S. Zhang, Gain- and Loss-Induced Topological Insulating Phase in a Non-Hermitian Electrical Circuit, Phys. Rev. Appl. **13**, 014047 (2020).
[34] A. J. Heeger, S. Kivelson, J. R. Schrieffer, and W. P. Su, Solitons in conducting polymers, Rev. Mod. Phys. **60**, 781 (1988).
[35] See Supplemental Material at http://link.aps.org/supplemental/10.1103/PhysRevLett.131.083801 for experimental and numerical methods as well as a theoretical symmetry classification of topology, which also includes Refs. [36–38].
[36] S. Ryu, A. P. Schnyder, A. Furusaki, and A. W. W. Ludwig, Topological insulators and superconductors: Tenfold way and dimensional hierarchy, New J. Phys. **12**, 065010 (2010).
[37] A. Kitaev, Periodic table for topological insulators and superconductors, AIP Conf. Proc. **1134**, 22 (2009).
[38] J. R. Pierce, Coupling of modes of propagation, J. Appl. Phys. **25**, 179 (1954).
[39] Z. Fedorova, C. Dauer, A. Sidorenko, S. Eggert, J. Kroha, and S. Linden, Dissipation engineered directional filter for quantum ratchets, Phys. Rev. Res. **3**, 013260 (2021).
[40] A. Drezet, A. Hohenau, D. Koller, A. Stepanov, H. Ditlbacher, B. Steinberger, F. Aussenegg, A. Leitner, and J. Krenn, Leakage radiation microscopy of surface plasmon polaritons, Mater. Sci. Eng. B **149**, 220 (2008).
[41] S. Longhi, Zak phase of photons in optical waveguide lattices, Opt. Lett. **38**, 3716 (2013).
[42] Z. Fedorova, H. Qiu, S. Linden, and J. Kroha, Observation of topological transport quantization by dissipation in fast Thouless pumps, Nat. Commun. **11**, 3758 (2020).
[43] C. Kurtscheid, D. Dung, A. Redmann, E. Busley, J. Klaers, F. Vewinger, J. Schmitt, and M. Weitz, Realizing arbitrary trapping potentials for light via direct laser writing of mirror surface profiles, Europhys. Lett. **130**, 54001 (2020).
[44] E. Busley, L. E. Miranda, A. Redmann, C. Kurtscheid, K. K. Umesh, F. Vewinger, M. Weitz, and J. Schmitt, Compressibility and the equation of state of an optical quantum gas in a box, Science **375**, 1403 (2022).
[45] J. Schmitt, T. Damm, D. Dung, F. Vewinger, J. Klaers, and M. Weitz, Observation of Grand-Canonical Number Statistics in a Photon Bose-Einstein Condensate, Phys. Rev. Lett. **112**, 030401 (2014).